Volume 15
Number 19
21 May 2024
Pages 6981–7360

Chemical Science

rsc.li/chemical-science

ISSN 2041-6539

ROYAL SOCIETY OF CHEMISTRY

EDGE ARTICLE

Takahiro Ichikawa, Takeshi Yamada *et al.*
Surface proton hopping conduction mechanism dominant polymer electrolytes created by self-assembly of bicontinuous cubic liquid crystals

Chemical Science

ROYAL SOCIETY OF CHEMISTRY

EDGE ARTICLE

View Article Online
View Journal | View Issue

Cite this: *Chem. Sci.*, 2024, **15**, 7034

All publication charges for this article have been paid for by the Royal Society of Chemistry

Received 20th February 2024
Accepted 8th April 2024

DOI: 10.1039/d4sc01211a

rsc.li/chemical-science

Surface proton hopping conduction mechanism dominant polymer electrolytes created by self-assembly of bicontinuous cubic liquid crystals†

Takahiro Ichikawa, *[a] Takeshi Yamada, *[b] Nanami Aoki,[a] Yuki Maehara,[a] Kaori Suda[a] and Tsubasa Kobayashi [a]

For the development of the next generation of fuel cells, it is essential to create an innovative design principle of polymer electrolytes that is beyond extension of the existing strategy. In the present study, we focused on the surface hopping proton conduction mechanism where an activation energy for proton conduction is greatly reduced by decreasing the distance between SO_3^- groups. Our gyroid nanostructured polymer film (**Film-G**), with a hydrophilic surface where the SO_3^- groups are aligned densely and precisely, shows high proton conductivity of the order of 10^{-2} S cm^{-1} when the water content is about 15 wt%. We reveal that the high proton conductivity of **Film-G** is attributed to the exhibition of an extremely-fast surface hopping conduction mechanism due to the reduced activation energy barrier along the gyroid minimal surface. This finding should introduce a game-changing novel opportunity in polymer electrolyte design.

Introduction

Nafion, which was developed in the late 1960s by DuPont, is surely the most successful polymer electrolyte because of its advanced proton conductivity and high mechanical stability.[1–3] Significant efforts have been made for several decades to develop proton conductive polymer electrolytes beyond Nafion;[4] however, Nafion still reigns as the most commonly used polymer electrolyte membrane for fuel cells and some other applications.[3] Proton conduction in Nafion can be understood using a simple 2D nanochannel model composed of a water nanochannel sandwiched between hydrophobic walls (Fig. 1a).[5,6] There are three proton conduction mechanisms in the nanochannel. One is the Grotthuss mechanism,[7] which is a mechanism to transport protons *via* the formation/cleavage of hydrogen-bonding networks of water molecules in the bulk water region, namely a water pool, in the center of the nanochannel. The second is the en masse diffusion mechanism, which is the mechanism whereby hydrated oxonium ions migrate in the water pool. The third one is the surface proton hopping conduction (SPHC) mechanism where there are proton hops (PHs) from an SO_3^- site on the surface of the hydrophobic wall to the neighboring SO_3^- site *via* bridging water molecules between them. The proton conductivities in each mechanism are represented by σ^G, σ^E, and σ^{Σ}, respectively. The total proton conductivity of the polymer electrolyte membranes is $\sigma^G + \sigma^E + \sigma^{\Sigma}$. Because of the significantly high proton conductivity in the Grotthuss mechanism, it has been common sense that the construction of macroscopically-continuous water pools, to

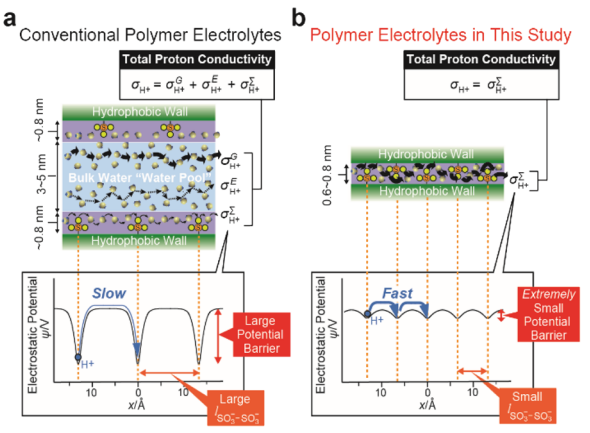

Fig. 1 (a) Schematic representation of a proton conductive water nanochannel with a thickness of several nanometers. Grotthuss conduction (σ^G) is the dominant proton conduction mechanism. It is a useful model for conventional proton conductive polymer electrolytes, such as Nafion. (b) Schematic representation of a proton conductive water nanosheet with a thickness of <1 nm. Surface proton hopping conduction (σ^{Σ}) is the dominant conduction mechanism. Electrostatic potentials in the plane parallel to the hydrophobic wall surface are described.

[a]*Department of Biotechnology and Life Science, Tokyo University of Agriculture and Technology, Naka-cho, Koganei, Tokyo, 184-8588, Japan. E-mail: t-ichi@cc.tuat.ac.jp*
[b]*Neutron Science and Technology Center, Comprehensive Research Organization for Science and Society, Tokai, Ibaraki, 319-1106, Japan*

† Electronic supplementary information (ESI) available. See DOI: https://doi.org/10.1039/d4sc01211a

enhance the contribution of σ^{G}, is the most important design principle for creating advanced proton conductive polymer electrolytes.

Here, we propose a totally new design principle departing from the common sense idea for the creation of proton conductive polymer electrolytes showing high proton conductivity. We focused on the theoretical foresight on the SPHC mechanism. In 2001, Eikerling *et al.* revealed that distances between the neighboring SO_3^- groups ($l_{SO_3^-\text{–}SO_3^-}$) on a hydrophobic wall surface strongly influence the electrostatic potential barrier in a direction parallel to the hydrophobic wall surface, ψ (Fig. 1a).[5] According to their estimates, when $l_{SO_3^-\text{–}SO_3^-} = 15$ Å, ψ is about 30 kJ mol^{-1} while it reduces exponentially to 2–3 kJ mol^{-1} as $l_{SO_3^-\text{–}SO_3^-}$ decreases to 5 Å. Since $l_{SO_3^-\text{–}SO_3^-}$ values in Nafion are relatively large at approximately 12 to 20 Å,[3,5] the ψ in Nafion is considered to be very large and consequently the σ^{Σ} of Nafion appears as a very small value. These insights have led many researchers to consider the SPHC mechanism to be trivial; however, we envision that the dense and highly periodic alignment of SO_3^- sites on a continuous surface should enable an ultrafast SPHC mechanism with an extremely small electrostatic potential barrier, resulting in the exhibition of a high proton conductivity on the order of 10^{-2} to 10^{-1} S cm^{-1}, that is, comparable to σ^{G} in Nafion and/or bulk water (Fig. 1b). Recently, the number of studies on the design of advanced proton conductive materials focusing on the alignment of the SO_3^- groups has been increasing.[8–15] Moreover, there are some studies that focus on the importance of the SPHC mechanism.[16,17] There are also some studies that have employed the potential utility of zwitterions as ion conductive materials.[18–20] Even bearing these previous studies in mind, the present work is the first study in which high proton conductivity is induced solely by the SPHC mechanism with an extremely-small activation energy.

Results and discussion

Aiming for the construction of polymer electrolytes with a dense and highly periodic alignment of SO_3^- sites for the SPHC mechanism, we focused on our previously-designed liquid-crystalline (LC) amphiphile **GZ** (Fig. 2a).[21] **GZ** has an ability to co-organize into bicontinuous cubic (Cub_{bi}) phases with some acids, such as bis(trifluoromethane)sulfonimide (HTf_2N) (Fig. 2b) and a small amount of water. In the Cub_{bi} phase, all of the SO_3^- groups of **GZ** are aligned on a 3D gyroid minimal surface (G-surface) in a cubic cell with a lattice parameter (L_{Cubic}) of approximately 9–10 nm. A significant point is that it is possible to preserve its unique molecularly assembled nanostructure by *in situ* polymerization, which yields a self-standing polymer film, **Film-G**, with gyroid nanostructures (Fig. 2c). We roughly calculated $l_{SO_3^-\text{–}SO_3^-}$ in **Film-G** containing X wt% of water (**Film-G(X)**) based on structural analysis and its physicochemical properties (Fig. S2†). $l_{SO_3^-\text{–}SO_3^-}$ in **Film-G(16.4)** was estimated to be roughly 5.9 Å (Fig. 2d and S3†), which is predominantly shorter than that in Nafion. This is a value for which one can expect the exhibition of an ultrafast SPHC mechanism with a very small electrostatic potential barrier, ψ.

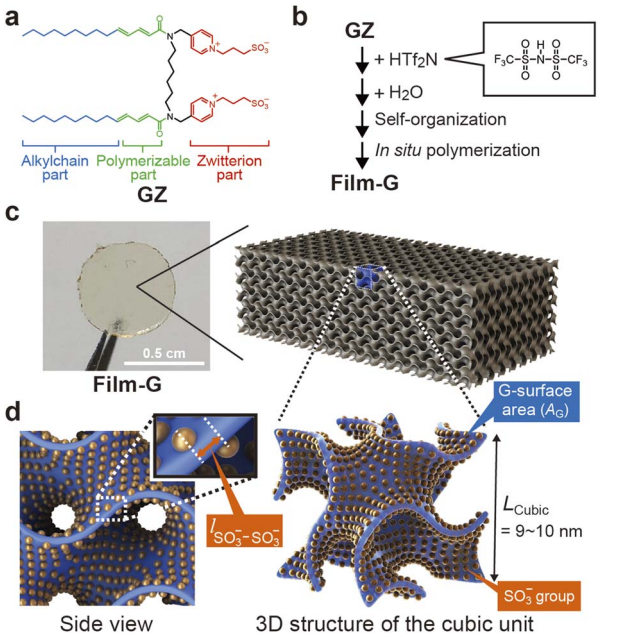

Fig. 2 (a) Molecular structure of amphiphilic zwitterion monomer **GZ**. (b) Preparation scheme for a gyroid nanostructured polymer film (**Film-G**). (c) A photograph of **Film-G** and 3D image of the gyroid nanostructure in **Film-G**. (d) 3D image of a cubic cell in **Film-G**. A water nanosheet is constructed along a gyroid minimal surface (G-surface) shown in blue. The positions of the SO_3^- groups of **GZ** are displayed as orange spheres.

We expect that SPHC mechanisms in **Film-G** with $l_{SO_3^-\text{–}SO_3^-} = 5.9$ Å can be roughly classified into four types depending on the degree of hydration of the SO_3^- groups (Fig. 3a–d). In the driest state, SPHC is composed only of very slow PHs due to the strong

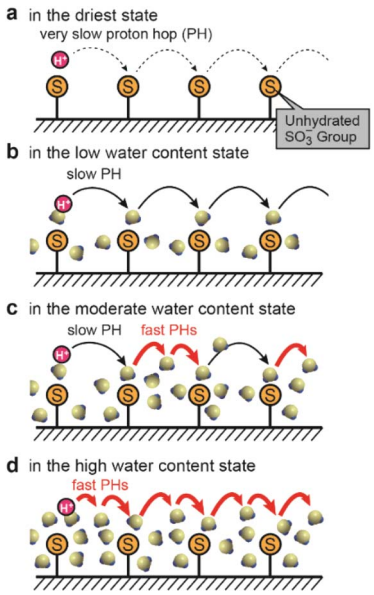

Fig. 3 Schematic illustration of the SPHC mechanism on the G-surface in **Film-G** with various water contents: (a) in the driest state; (b) in low water content; (c) in moderate water content; and (d) in high water content.

electrostatic interaction between the SO_3^- anion and a proton (Fig. 3a). In the low-water-content state, these PHs are slightly accelerated due to the hydration of the SO_3^- groups that largely weakens SO_3^-–proton interactions, while the PH speed is still slow because $l_{SO_3^-\text{–}SO_3^-} = 5.9$ Å is a large value for a proton to hop directly (Fig. 3b). A further increase in water content leads to the situation where two hydrated SO_3^- groups are connected *via* bound water molecules. PHs *via* these hydrated SO_3^- groups are greatly accelerated, while PHs *via* those with fewer bound water molecules are still slow (Fig. 3c). When the water content reaches a situation where all the SO_3^- groups are connected by bound water molecules (Fig. 3d), all PHs are highly activated and an effective SPHC mechanism is enabled at a macroscopic scale. This expectation is consistent with the dependence of proton conductivity (σ_{H^+}) of **Film-G** on water content that was reported in our previous study.[21]

When the SPHC is dominant in proton conductivity, its σ_{H^+} can be described by

$$\sigma_{H^+} = \frac{\varepsilon_i}{\theta}\frac{F^2}{RT}\left(D_{H^+}^{\Sigma} C_{H^+}^{\Sigma}\right) \quad (1)$$

where F is Faraday's constant, R is the universal gas constant, $D_{H^+}{}^{\Sigma}$ ($cm^2\ s^{-1}$) and $C_{H^+}{}^{\Sigma}$ ($mol\ cm^{-3}$) are the diffusion coefficient and the concentration of H^+ on the surface, T (K) is temperature, ε_i (dimensionless) is the volume fraction occupied by water, and θ (dimensionless) is a tortuosity factor. Detailed discussion about these parameters is provided in the ESI.† We will discuss below whether the high σ_{H^+} of **Film-G** can be explained solely by the SPHC mechanism.

According to the view of random walk diffusion, $D_{H^+}{}^{\Sigma}$ is given by the Einstein–Smoluchowski equation[22,23]

$$D_{H^+}^{\Sigma} = \frac{l_{\Sigma}^2}{\kappa \tau_D^{\Sigma}} \quad (2)$$

where κ is a constant value that depends on the dimensionality of random proton hops, l_Σ is the hopping length, and τ_D^{Σ} is the mean jump time for a PH. τ_D^{Σ} can be expressed as

$$\tau_D^{\Sigma} = {\nu_0}^{-1} \exp\left(\frac{\Delta G_{\Sigma}^{e,0}}{k_B T}\right) \quad (3)$$

where ν_0 is the thermal frequency, k_B is the Boltzmann constant, and $\Delta G_{\Sigma}^{e,0}$ is the effective Gibbs free energy of activation for surface hops. ν_0 is expressed as $\frac{k_B T}{h}$, where h is Planck's constant. The main component of $\Delta G_{\Sigma}^{e,0}$ is the potential barrier in the SPHC mechanism.[5] Assuming that the proton conduction in **Film-G(X)** is solely based on the SPHC mechanism, $\Delta G_{\Sigma}^{e,0}$ was estimated to be 13.3 kJ mol^{-1} for **Film-G(15.2)** using the experimental value of $\sigma_{H^+} = 8.5 \times 10^{-3}$ S cm^{-1} (Tables S4 and S5†). To confirm the validity of $\Delta G_{\Sigma}^{e,0} = 13.3$ kJ mol^{-1}, we examined the activation energy (E_a) of **Film-G(X)**. The temperature dependences of σ_{H^+} of **Film-G(15.2)**, **Film-G(9.9)**, and **Film-G(6.0)** are shown in Fig. 4 using an Arrhenius plot. The measurements were performed in a narrow temperature range of 30 to 40 °C under a constant relative humidity of 90% with the aim of reducing the change in water content during the measurements. E_a was found to be 17.2 kJ mol^{-1} for **Film-G(15.2)**, which was close enough to $\Delta G_{\Sigma}^{e,0} = 13.3$ kJ mol^{-1}. Since there is a small increase in the water content in **Film-G(15.2)** upon heating from 30 to 40 °C when the sample is kept under RH = 90% due to the increase in the absolute humidity, E_a = 17.2 kJ mol^{-1} is expected to be an overestimate. The exact value of E_a should be slightly smaller than 17.2 kJ mol^{-1}, meaning that our estimate of $\Delta G_{\Sigma}^{e,0} = 13.3$ kJ mol^{-1} is very reasonable. These results strongly support the validity of our assumption that the SPHC mechanism is solely-dominant for the proton conduction mechanism in **Film-G(15.2)**. Conversely, larger values of $E_a = 26.8$ and 35.3 kJ mol^{-1} were found for **Film-G(9.9)** and **Film-G(6.0)**, respectively, with lower water contents. This can be explained by the situation, where the SO_3^- groups are partially bridged with bound water molecules, as shown in Fig. 3c, and some PHs with slower speed exist along the G-surface. This indicates that a suitable amount of water molecules is required to exclude slow PHs and yield only fast PHs, leading to the exhibition of high proton conductivity at a macroscopic scale.

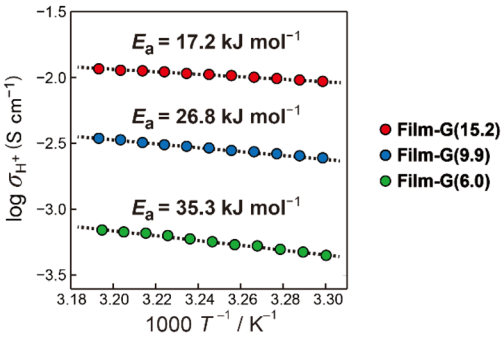

Fig. 4 Experimentally-obtained σ_{H^+} values of Film-G(15.2), Film-G(9.9), and Film-G(6.0) plotted against the reciprocal of absolute temperature.

Here, we compare the estimated physical property values of **Film-G** with those of Nafion. Using the value of $\Delta G_{\Sigma}^{e,0}$ = 13.3 kJ mol^{-1}, the $D_{H^+}{}^{\Sigma}$ of **Film-G(15.2)** is calculated to be 6.99×10^{-6} $cm^2\ s^{-1}$, which is 70 times larger than that in Nafion.[6] The ultrafast SPHC in **Film-G(15.2)** is ascribed to the formation of a considerably reduced electrostatic potential barrier on the G-surface by the correlated barrier hopping model[24] that was realized for the first time by creating a unique situation, where the SO_3^- groups are placed on a continuous surface in a dense and highly-periodic manner.

The experimental results on the water composition dependence of the σ_{H^+} of **Film-G** indicated that it is necessary to introduce a suitable amount of water molecules on the SO_3^--aligned surface to enable the SPHC mechanism with a reduced ψ. We expected that the elucidation of the water state, dynamics and their composition dependence should be a significant way to understand the proton conduction mechanism in **Film-G(X)**. The state of water in **Film-G(X)** was examined by DSC measurements (Fig. 5 and S11†). The DSC thermograms on cooling are shown in Fig. 5. There is no exothermic peak corresponding to the crystallization of water when the water content X is 17.3 wt% or less, while a small exothermic peak is

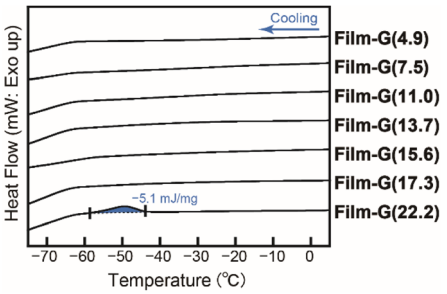

Fig. 5 DSC thermograms of **Film-G(X)** on cooling. *X* is the water content in the film (wt%).

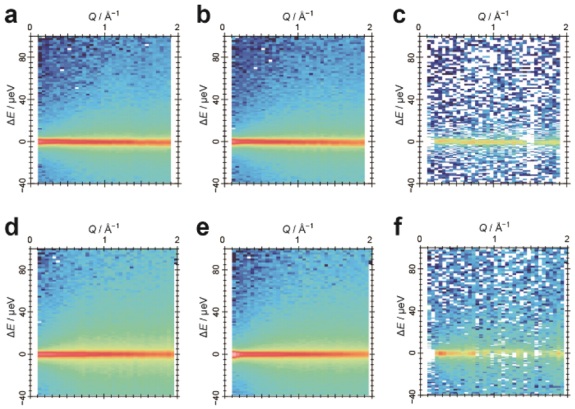

Fig. 6 Contour maps of QENS data of (a) **Film-G**/3H_2O and (b) **Film-G**/3D_2O at 300 K. (c) A differential contour map between **Film-G**/3H_2O and **Film-G**/3D_2O. Contour maps of QENS data of (d) **Film-G**/6H_2O and (e) **Film-G**/6D_2O at 300 K. (f) A differential contour map between **Film-G**/6H_2O and **Film-G**/6D_2O.

observed when $X = 22.2$ wt%. These results clearly suggest that the water molecules in **Film-G(X)** exist as non-freezing bound water at least when $X \leq 17.3$, suggesting that the ultrafast SPHC mechanism in **Film-G(15.2)** is assisted only by non-freezing bound water.

With the aim of further investigating the dynamics of water in **Film-G(X)**, we focused on quasi-elastic neutron scattering (QENS) measurements. QENS is a powerful technique for investigating the dynamics of water molecules in the picosecond to nanosecond timeframe and Ångstrom length-scale due to the large incoherent scattering cross-section of hydrogen. It has been employed for various materials including Nafion to reveal the dynamics of water molecules in it.[25,26] Unlike Nafion that is mainly composed of C, O, S, and F elements, **Film-G** contains many hydrogen atoms. Thus, to obtain information on the dynamics of the water molecules in **Film-G**, we planned to examine the difference between the QENS spectra of **Film-G** containing normal water (H_2O) and those of **Film-G** containing heavy water (D_2O). Two types of **Film-G** samples with moderate water content (9.0 wt% (**Film-G(9.0)**)) and high water content (16.4 wt% (**Film-G(16.4)**)) were prepared by putting them under controlled relative humidity conditions. Resultant polymer films contain 3.0 and 6.0 water molecules per SO_3^- group, respectively. Below they are described as **Film-G**/$m$$H_2O$ ($m = 3$ and 6). Using D_2O, **Film-G**/$m$$D_2O$ ($m = 3$ and 6) were also prepared.

QENS experiments were carried out for these four samples at 300, 280, 260, and 240 K. The same experiment was performed at 10 K for resolution. Contour maps of QENS data of **Film-G**/3H_2O and **Film-G**/3D_2O at 300 K are shown in Fig. 6a and b. *X*- and *Y*-axes are momentum transfer (Q) and energy transfer (ΔE), respectively. ΔE reflects the quantity of energy exchange between an incident neutron and the sample. If a sample shows a relaxation phenomenon, a broad peak is observed as QENS around the elastic position ($\Delta E = 0$). The width of the QENS broadening is inversely proportional to the relaxation time.[27] There is a strong sharp scattering intensity at $\Delta E = 0$, and a moderate broad scattering intensity centered at $\Delta E = 0$, indicating that elastic and quasi-elastic components exist in the films. To extract the information on water molecules in **Film-G**, a differential contour map between the two was created using a scaling factor derived from the weight ratio of the two samples in the dry state (Fig. 6c). In the differential contour map, a significant difference is found mostly only in the $\Delta E = 0$ region, indicating that the dynamics of the water molecules in **Film-G**/3H_2O have almost stopped or are slower than the timescale represented by the instrumental energy resolution. Conversely, completely different results were obtained when $m = 6$. The contour maps of the QENS data of **Film-G**/6H_2O and **Film-G**/6D_2O and their differential data are shown in Fig. 6d–f. It is noteworthy that a broad scattering intensity was found in Fig. 6f, indicating that there is a certain amount of mobile water molecules in **Film-G**/6H_2O.

To evaluate the dynamics of the water molecules in **Film-G** more quantitatively, we analyzed the QENS profiles of **Film-G**/$m$$D_2O$ and **Film-G**/$m$$H_2O$ ($m = 3$ and 6). The QENS profiles of $m = 3$ were integrated in the Q direction due to the small contribution from hydrated water. The obtained results were fitted by the following phenomenological equation

$$S(Q,E) = \left\{ A_0\delta(E) + \sum_{i=1}^{n} A_i L_i(\Gamma_i, E) \right\} \otimes R(Q,E) \qquad (4)$$

where $A_0\delta(E)$ denotes the elastic component with coefficient A_0 and delta-function $\delta(E)$, A_i is the coefficient of the i-th Lorentzian-function, $L_i(\Gamma_i,E)$, where Γ_i is the half width at half maximum (HWHM) of the Lorentzian-function, and $R(Q,E)$ refers to the instrumental resolution function, which was obtained at 10 K. Fig. 7a and b show fitting results for the QENS profile of **Film-G**/3D_2O and **Film-G**/6D_2O at $T = 300$ K. It is successfully fitted with the sum of a delta-function and two Lorentzian-functions ($n = 2$ in eqn (4)), which are drawn with lines in red, green, and blue, respectively. Since D_2O hardly contributes to the QENS profile, the observed QENS broadening reflects the dynamics of **Film-G**, namely the alkyl chain motion of **GZ** (Fig. S16–S18†). In contrast, the QENS profile of **Film-G**/$m$$H_2O$ ($m = 3$ and 6) includes dynamics of not only **Film-G** but also $m$$H_2O$. This difference between **Film-G**/$m$$H_2O$ and **Film-G**/$m$$D_2O$ (Fig. 6c and f) leads us to consider that an additional Lorentzian-function, representing the mobile water molecules, is required for fitting of the QENS profile of **Film-G**/$m$$H_2O$.

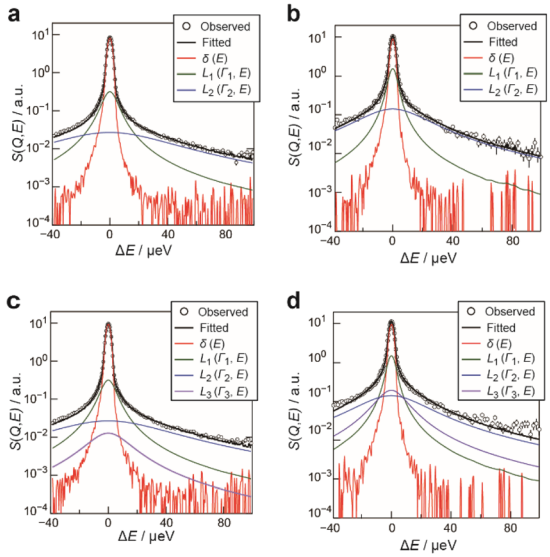

Fig. 7 (a) Fitting of the observed QENS profile of **Film-G**/3D_2O with the sum of a delta function and two Lorentzian-functions convoluted with the resolution function. (b) Fitting of the observed QENS profile of **Film-G**/6D_2O at Q = 0.78 Å^{-1} and 300 K with the sum of a delta function and two Lorentzian-functions convoluted with the resolution function. (c) Fitting of the QENS profile of **Film-G**/3H_2O when the parameters of two Lorentzian-functions were fixed by the results of **Film-G**/3D_2O. (d) Fitting of the QENS profile of **Film-G**/6H_2O at Q = 0.78 Å^{-1} and 300 K when the parameters of two Lorentzian-functions were fixed by the results of **Film-G**/6D_2O.

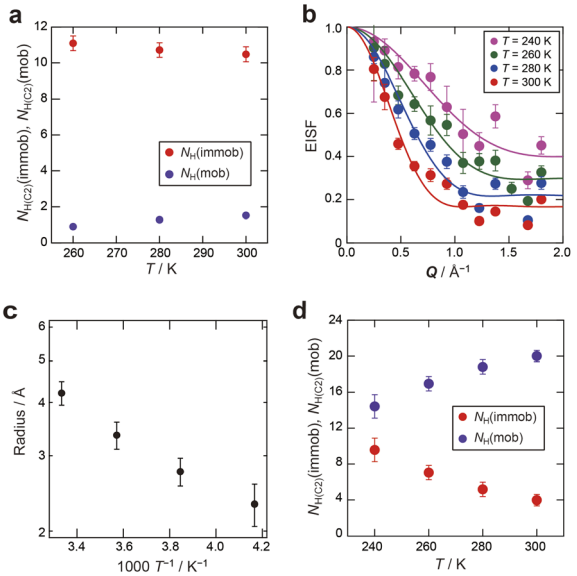

Fig. 8 (a) Number of immobile and mobile hydrogen atoms ($N_{H(immob)}$ and $N_{H(mob)}$) in 3H_2O. (b) Q dependence of EISF of 6H_2O in **Film-G**/6H_2O. The solid lines are results fitted with eqn (8). (c) Temperature dependence of the radius of the confined sphere obtained from the fitted results of the EISF (b). (d) Number of immobile and mobile hydrogen atoms ($N_{H(immob)}$ and $N_{H(mob)}$) in 6H_2O.

Therefore, it was fitted by eqn (4) with three Lorentzian-functions (n = 3), where parameters L_1 and L_2 corresponding to **Film-G** were fixed using the results of **Film-G**/$m$$D_2O$, and the three parameters A_0, A_3, and Γ_3 were adjusted. This approach substantially reproduced observed data (Fig. 7c and d).

In the case of m = 3, the number of immobile and mobile hydrogen atoms ($N_{H(immob)}$ and $N_{H(mob)}$) in **Film-G**/3H_2O was estimated as follows,

$$N_H(\text{immob}) = \frac{A_0(\textbf{Film-G}/3H_2O) - A_0(\textbf{Film-G}/3D_2O)}{(A_0(\textbf{Film-G}/3H_2O) - A_0(\textbf{Film-G}/3D_2O) + A_3)} \times 12 \quad (5)$$

$$N_H(\text{mob}) = \frac{A_3}{(A_0(\textbf{Film-G}/3H_2O) - A_0(\textbf{Film-G}/3D_2O) + A_3)} \times 12 \quad (6)$$

where 12 indicates the number of hydrogen atoms in the water molecules per **GZ** molecule. The obtained $N_{H(immob)}$ and $N_{H(mob)}$ are plotted in Fig. 8a. It is notable that immobile water predominates in **Film-G**/3H_2O. In the case of m = 3, the hydration degree on the G-surface is expected to be the situation shown in Fig. 3b or c. Therefore, many of the water molecules are fixed on the SO_3^- groups, while some of them near H^+ are fluctuating.

In contrast, in the case of m = 6, since it was revealed that a certain amount of the water molecules are in the mobile state, the Q dependence of the parameter L_3 was examined to extract spatial information about the observed dynamics. The Q dependence of Γ_3 at 300 K did not approach zero at Q = 0 Å^{-1} (Fig. S20†). Although obtained data was scattered, Γ_3 was found to be almost constant with respect to Q. These results suggest that the observed dynamics corresponding to L_3 is a local mode, such as rotation and/or local jumps of the water molecules. A similar trend was also observed at other temperatures. This means the scale of the localized mode is within a scale of several Ångstroms. For further consideration, the Q dependence of the elastic incoherent scattering factor (EISF) was calculated as follows,

$$\text{EISF}(Q) = \frac{A_0(\textbf{Film-G}/6H_2O) - A_0(\textbf{Film-G}/6D_2O)}{(A_0(\textbf{Film-G}/6H_2O) - A_0(\textbf{Film-G}/6D_2O) + A_3)} \quad (7)$$

The Q dependence of EISF, as plotted in Fig. 8b, was well reproduced by a diffusion model in the confined sphere,[28] as follows,

$$\text{EISF}(Q) = (1 - f_{\text{mob}}) + f_{\text{mob}}\left\{\frac{3j_1(Qr)}{Qr}\right\}^2 \quad (8)$$

where f_{mob}, r, and j_1 are the mobile fraction of hydrogen corresponding to water, the radius of the confined sphere, and a first-order spherical Bessel function, respectively. The value of r was 4.2 Å at 300 K (Fig. 8c), which covers enough neighboring sites of SO_3^- ($l_{SO_3^- - SO_3^-}$). The space decreased with decreasing temperature. $N_{H(immob)}$ and $N_{H(mob)}$ were estimated from 24 × (1 − f_{mob}) and 24 × f_{mob}, respectively (Fig. 8d). In contrast to **Film-G**/3H_2O, the mobile water predominates in **Film-G**/6H_2O. In the case of m = 6, the degree of hydration reaches the

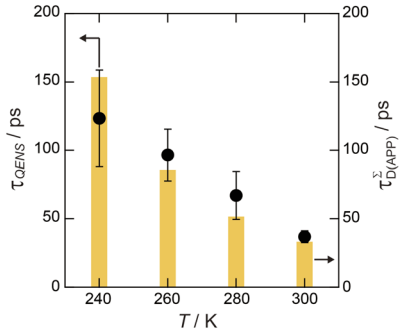

Fig. 9 Relaxation time of mobile water molecules (τ_{QENS}) estimated from the HWHM of L_3 in $6H_2O$. τ_D^{Σ} values of **Film-G(15.2)** at various temperatures are also shown in the yellow bar graph.

situation shown in Fig. 3d, where the presence of H^+ causes not only the near water molecules to wobble but also distant ones connected through hydrogen-bonding networks, which consequently puts a large part of the water molecules in a mobile state.

The relaxation time of these mobile water molecules (τ_{QENS}) was evaluated using the following formula,

$$\tau_{QENS} = \hbar \frac{1}{\Gamma_3} \quad (9)$$

where $\hbar$ is $h/2\pi$. The value τ_{QENS} was estimated to be 37 ± 4 ps at 300 K, which is of the same order as τ_D^{Σ} calculated when assuming $\Delta G_{\Sigma}^{e,0} = 13.3$ kJ mol^{-1} (Table S5†). Consistency of theoretical τ_D^{Σ} and experimental τ_{QENS} is also found for results at other temperatures (Fig. 9). These results suggest that the dynamics of the mobile water molecules are deeply involved in the SPHC mechanism.

Conclusions

We have succeeded in demonstrating the potential utility of the surface proton hopping conduction (SPHC) mechanism for the development of advanced proton conductive polymer electrolytes. These findings will contribute to the development of advanced fuel cells, such as anhydrous-drive-type and/or low-temperature-drive-type ones. From a comprehensive viewpoint, present findings suggest that control over self-organization should be a key strategy for creating new functional materials that support next-generation technologies.

Data availability

The datasets supporting this article have been uploaded as part of the ESI.†

Author contributions

T. I. supervised this project. T. I. and T. K. designed materials. T. I., N. A., Y. M., K. S., T. K., and T. Y. performed the experiments and analyzed the data. T. I. and T. Y. wrote the manuscript. All authors discussed the results and commented on the manuscript. All authors have given approval to the final version of the manuscript.

Conflicts of interest

There are no conflicts to declare.

Acknowledgements

This work was supported by the Japan Science and Technology Agency (JST) FOREST (JPMJFR223C). This work was also supported by JSPS KAKENHI numbers JP21H02010, JP22H04526, and JP23K17937 from the Japan Society for the Promotion of Science. This work was partially supported by Nippon Sheet Glass Foundation for Materials Science and Engineering. The QENS experiments at the Materials and Life Science Experimental Facility of the J-PARC was performed under a user program (Proposal No. 2022A0005 and 2023A0072).

Notes and references

1 K.-D. Kreuer, *Chem. Mater.*, 1996, **8**, 610–641.
2 K. A. Mauritz and R. B. Moore, *Chem. Rev.*, 2004, **104**, 4535–4586.
3 A. Kusoglu and A. Z. Weber, *Chem. Rev.*, 2017, **117**, 987–1104.
4 T. J. Peckham and S. Holdcroft, *Adv. Mater.*, 2010, **22**, 4667–4690.
5 M. Eikerling and A. A. Kornyshev, *J. Electroanal. Chem.*, 2001, **502**, 1–14.
6 P. Choi, N. H. Jalani and R. Datta, *J. Electrochem. Soc.*, 2005, **152**, E123–E130.
7 N. Agmon, *Chem. Phys. Lett.*, 1995, **244**, 456–462.
8 T. Kato, M. Yoshio, T. Ichikawa, B. Soberats, H. Ohno and M. Funahashi, *Nat. Rev. Mater.*, 2017, **2**, 17001.
9 S. Ueda, J. Kagimoto, T. Ichikawa, T. Kato and H. Ohno, *Adv. Mater.*, 2011, **23**, 3071–3074.
10 T. Ichikawa, T. Kato and H. Ohno, *J. Am. Chem. Soc.*, 2012, **134**, 11354–11357.
11 Y. Chen, M. Thorn, S. Christensen, C. Versek, A. Poe, R. C. Hayward, M. T. Tuominen and S. Thayumanavan, *Nat. Chem.*, 2010, **2**, 503–508.
12 G. L. Jackson, D. V. Perroni and M. K. Mahanthappa, *J. Phys. Chem. B*, 2017, **121**, 9429–9436.
13 Y. Nagao, *Langmuir*, 2017, **33**, 12547–12558.
14 E. B. Trigg, T. W. Gaines, M. Maréchal, D. E. Moed, P. Rannou, K. B. Wagener, M. J. Stevens and K. I. Winey, *Nat. Mater.*, 2018, **17**, 725–731.
15 D.-W. Lim and H. Kitagawa, *Chem. Soc. Rev.*, 2021, **50**, 6349–6368.
16 C. Yin, J. Li, Y. Zhou, H. Zhang, P. Fang and C. He, *ACS Appl. Mater. Interfaces*, 2018, **10**, 14026–14035.
17 M. Tanaka, *Polym. J.*, 2016, **48**, 51–58.
18 M. Yoshizawa, M. Hirao, K. I. Akita and H. Ohno, *J. Mater. Chem.*, 2001, **11**, 1057–1062.
19 C. Tiyapiboonchaiya, *et al.*, *Nat. Mater.*, 2004, **3**, 29–32.
20 O. Kim, K. Kim, U. H. Choi and M. J. Park, *Nat. Commun.*, 2018, **9**, 5029.

21 T. Kobayashi, Y. Li, A. Ono, X.-b. Zeng and T. Ichikawa, *Chem. Sci.*, 2019, **10**, 6245–6253.
22 P. W. Atkins, *Physical Chemistry*, W. H. Freeman and Company, New York, 3rd edn, 1986.
23 J. Philibert, *Atom Movements Diffusion and Mass Transport in Solids*, Les Editions de Physique, Les Ulis, 1991.
24 Y. Ben Taher, *et al.*, *Appl. Phys. A*, 2015, **120**, 1537–1543.
25 J.-C. Perrin, S. Lyonnard and F. Volino, *J. Phys. Chem. C*, 2007, **111**, 3393–3404.
26 Q. Berrod, S. Hanot, A. Guillermo, S. Mossa and S. Lyonnard, *Sci. Rep.*, 2017, **7**, 8326.
27 M. Bée, *Quasielastic Neutron Scattering: Principles and Applications in Solid State Chemistry, Biology, and Materials Science*, Adam Hilger, Bristol, England, Philadelphia, 1988.
28 F. Volino and A. J. Dianoux, *Mol. Phys.*, 1980, **41**, 271.